Journal of Marine Research, 62, 771–786, 2004

Observed mechanisms of El Nino SST evolution in the Pacific

by P. Niiler[1], D.-K. Lee[2] and J. Moisan[3]

ABSTRACT

Tropical Pacific Ocean SST and velocity observations are used to construct NINO3 and NINO4 area average, 20-year long interannual time series of local and advective convergences of thermal energy. The variability of the sum of these observed convergences in each region is balanced by the vertical convergence of thermal energy due to the latent surface flux (86% in NINO3; 84% in NINO4). The latitude scale of the El Nino SST anomalies is shown to be equal to the ratio of the poleward mean speed of water parcels to the time scale at which thermal energy is given back to the atmosphere by a negative SST feedback through latent heat flux anomaly. Simultaneous observations and analyses of velocity and SST underscore the importance of the time-mean, wind-driven, poleward circulation in the establishment of the patterns of El Nino/SST anomalies directly north and south of the Pacific equator.

1. Introduction

During every "normal" year in the period of February to April the equatorial Pacific in the area 150E to 90W and 5N to 5S is relatively warm with sea-surface temperature (SST) of 27°C (±1°C). In the normal months of July–August an eastern basin cold *"tongue"* intensifies and a western basin *"pool"* warms to 30°C (Philander, 1990). When the surface expression of cold *tongue* is weak, SST stays in its warm mode, or El Nino condition exists, even though SST is not warmer than 30°C. The physical mechanisms that lead to the formation of El Nino condition are made manifest by understanding why water does not cool enough in the May–November period. If the ocean does not cool in the July–August period, the warming that occurred in the January–March does not go away and the state of the ocean is now considered an El Nino condition.

The mechanisms that produce the surface cold tongue in the tropics (Fig. 1) are small-scale vertical mixing of upwelled cold water from depth, horizontal advection of cold water from such a mixing region and an increased surface heat flux to the atmosphere. The dominating mechanisms depend upon the scales of interest. The large spatial scales of

1. Scripps Institution of Oceanography, University of California, 9500 Gilman Drive, La Jolla, California, 92093, U.S.A. ***email: pniiler@ucsd.edu***

2. Busan National University, Gumjeong-gu, 30 Jangjeon-dong, Busan 609-735, Republic of Korea.

3. NASA/GSFC, Laboratory for Hydrospheric Processes, Wallops Flight Facility, Wallops Island, Virginia, 23337-5099.

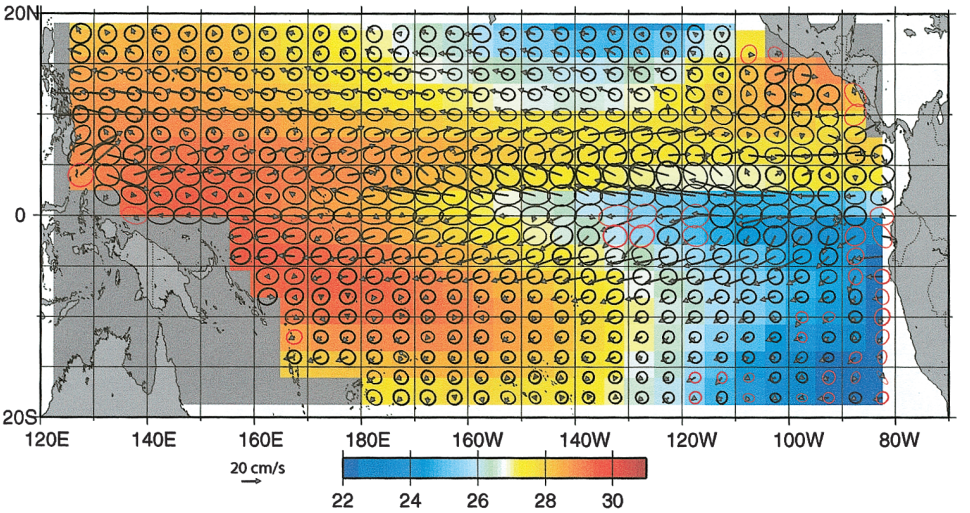

Figure 1. Mean velocity vectors and standard error ellipses drawn on mean SST distribution. The ellipses are red in areas of less than 40, 7-day average velocity observations. The standard error ellipses obeys the equation $(Nx'^2/\langle u'^2\rangle) + (Ny'^2/\langle v'^2\rangle) = 1$, where $(x', u'; y', v')$ are in the rotated coordinate system where $\langle u'v'\rangle = 0$; N is the number of independent observations.

5° latitude and 20° longitude are of interest to coupled ocean-atmosphere models for El Nino prediction because the tropical SST anomalies force the global atmosphere into an anomalous circulation very effectively on these scales (Philander, 1990). Here we demonstrate that on these large scales the time mean wind-driven Ekman currents are essential to a physically correct model of El Nino development with which the SST anomaly on the equator is transported poleward to fill the tropical Pacific.

In this paper we calculate and discuss the NINO3 (5S-5N, 150W-90W) and NINO4 (5S-5N, 160E-150W) area average thermal energy balances or the terms of the SST evolution equation on interannual time scales. We use satellite-tracked drifters and moored current meter observations of near-surface velocity and SST for calculating heat advection and COADS marine observations for calculating heat fluxes. We find that horizontal advection of the temperature anomaly by the time-mean velocity and the latent heat flux anomaly, as controlled by SST and winds, are the most important mechanisms in determining the interannual SST evolution averaged over both NINO3 and NINO4 regions. Wang and McPhaden (2000) demonstrated that on smaller spatial and temporal scales right on the equator, vertical turbulent processes also make important contributions.

2. Methodology of data treatment

a. The methodology

The objective is to estimate the left-hand side terms of the thermal balance equation from observations at the 15 m depth level and to construct a model for the right-hand side that has physical verity and is statistically supported by observations:

$$[\partial T/\partial t]' + [(V \cdot \nabla T)]' = [\partial Q/c\rho\partial z]'. \quad (1)$$

Here T is the near-surface bulk temperature, or SST, V is horizontal velocity at 15 m depth, [ ] denotes the spatial average over the NINO3 or NINO4 region, $\langle\ \rangle$ will denote the data ensemble or record length average and the prime, $'$, denotes the time variable component that has been low-pass filtered at 16 months. The spectral peak of the SST time series at the annual period has a band-width of about two months so a 16-month filter is used to remove the energy in the entire "annual band." The vertical convergence of the sum of turbulent and radiation fluxes at 15 m depth is $[\partial Q/\partial z]'$, a model for which will be developed in Section 3 in terms of the parameters that determine the surface flux and its vertical convergence; $c\rho$ is the sea-water heat capacity per unit volume.

Only the significant terms in the area average thermal energy balance on interannual time scales at 15 m-depth are shown in Eq. 1. The absence of the vertical gradient of temperature in the mixed layer inhibits vertical advection and thus $[(w\partial T/\partial z)]'$ does not appear. This "balance" at the 15 m level should not be confused with a "heat budget" or the vertical integral of the complete form of Eq. 1 through the entire vertical extent of the mixed layer where vertical advection processes are important in moving the base of the layer vertically (Swenson and Hansen, 1994). What is often considered as 'entrainment of cold water' in a budget equation does not appear explicitly in a balance equation, but is implicit in the term on the right-hand side of the equation in the parameterization of the vertical convergence of the turbulent component of the thermal energy flux.

The advection anomaly in Eq. (1) can be divided into three terms as follows:

$$[V \cdot \nabla T]' = [\langle V\rangle \cdot \nabla T']_A + [V' \cdot \nabla\langle T\rangle]_B + [V' \cdot \nabla T' + V'' \cdot \nabla T'']'_C, \quad (2)$$

where double prime represents all variations with periods shorter than 16 months. In the derivation of term C, it was assumed that the double prime and the prime terms are not correlated over the prime period of interest here.

Term A is the advective convergence of the SST anomaly due to the mean velocity and B is the advective convergence of the mean SST due to the anomalous velocity. The eddy term C has two components, one from the anomalies for periods shorter than 16 months and the second from anomalies for periods longer than 16 months. The reason for separating these fields was to point out that term A was typically the largest, and the component due to the northward mean advection of the anomaly was larger than that due to the eastward mean advection (Figs. 3, 4). Because the mean velocity and the spatial gradients of T' were well defined by our data, the interannual advection was well defined. The calculation of term C will be considered in more detail in Section 2d.

b. Data sets

The SST data are 1° × 1°, 7-day average Multi-Channel Sea Surface Temperature (MCSST) data distributed by National Center for Environmental Prediction (Reynolds and Smith, 1994; www.ncep.noaa.gov). The horizontal temperature gradients were computed by central finite differencing from these one-degree data and were spatially averaged in 1°

latitude × 5° longitude boxes. SST data cover the period of January 1, 1981–December 31, 2001.

The velocity data were derived from the drifters, including those that lost their drogues (Niiler, 2001), and current meter observations of 15 m depth velocity (Tropical Atmosphere Ocean {TAO} data at 165W; www.pmel.noaa.gov/tao). There were 67,264 weekly estimates of velocity from drifter data and 207 weekly estimates of velocity from TAO data within the NINO3,4 regions. These were averaged over one day and binned and averaged in time on 1° latitude × 5° longitude boxes for the same 7-day periods as the SST data. Velocity data cover the period January 1, 1988–December 31, 2001.

The heat flux data were derived from the Comprehensive Ocean-Atmosphere Data Set (COADS) January 1, 1950–December 31, 1989 time series of marine observations averaged on a 5° × 5° resolution with the methodology of Moisan and Niiler (1998). This methodology produces a seasonal cycle of fluxes that are in quantitative balance with the observed heat storage rate in the seasonal thermocline of the subtropical and subpolar North Pacific. The monthly net surface flux as well as the individual components were averaged over the NINO3 and NINO4 regions and then low passed at 16 months. These flux data will be used to develop a statistical model of the right-hand side of Eq. 1 as a function of SST and wind speed so the physics of the somewhat complicated air-sea interactions are made apparent.

c. The time-averaged fields

The time mean velocity and SST of the tropical Pacific (Fig. 1) display the familiar patterns of tropical Pacific currents and countercurrents, the western Pacific and Mexican warm *pools* and the east Pacific cold *tongue,* which is anchored to the west coast of South America. The time-mean velocity field was derived from 13 years of observations (158,345, 7-day vectors) and is well defined when compared to a conservative estimate of the standard error of the mean shown as ellipses (Niiler, 2001). This estimate uses 7 days as the Lagrangian de-correlation time scale, or independent estimates, for velocity along drifter tracks, which is an average value the time-scales computed locally from Lagrangian data (Bi, 1995). The vectors from 3° to 20° latitude show poleward components of velocity due to the wind-driven Ekman effects (Ralph and Niiler, 1999). These observed poleward currents are opposite to the direction of the equatorward surface geostrophic velocity relative to 1000 m or 3000 m depth (Wijffels *et al.,* 1997) and this difference turns out to be the crucial element in the El Nino near-surface thermal energy balance.

d. Analyses of time variability

The 16-month low-passed SST variance, which lies within 10° latitude of the equator (Fig. 2a), has a longitudinally extended maximum in the equatorial zone in both NINO3 and NINO4 regions. It is the goal of this analysis to explain what processes constrain the SST variance to develop only within 10° of the equator. It is well known that this interannual variance has large spatial coherence scales. The time evolving SST anomaly

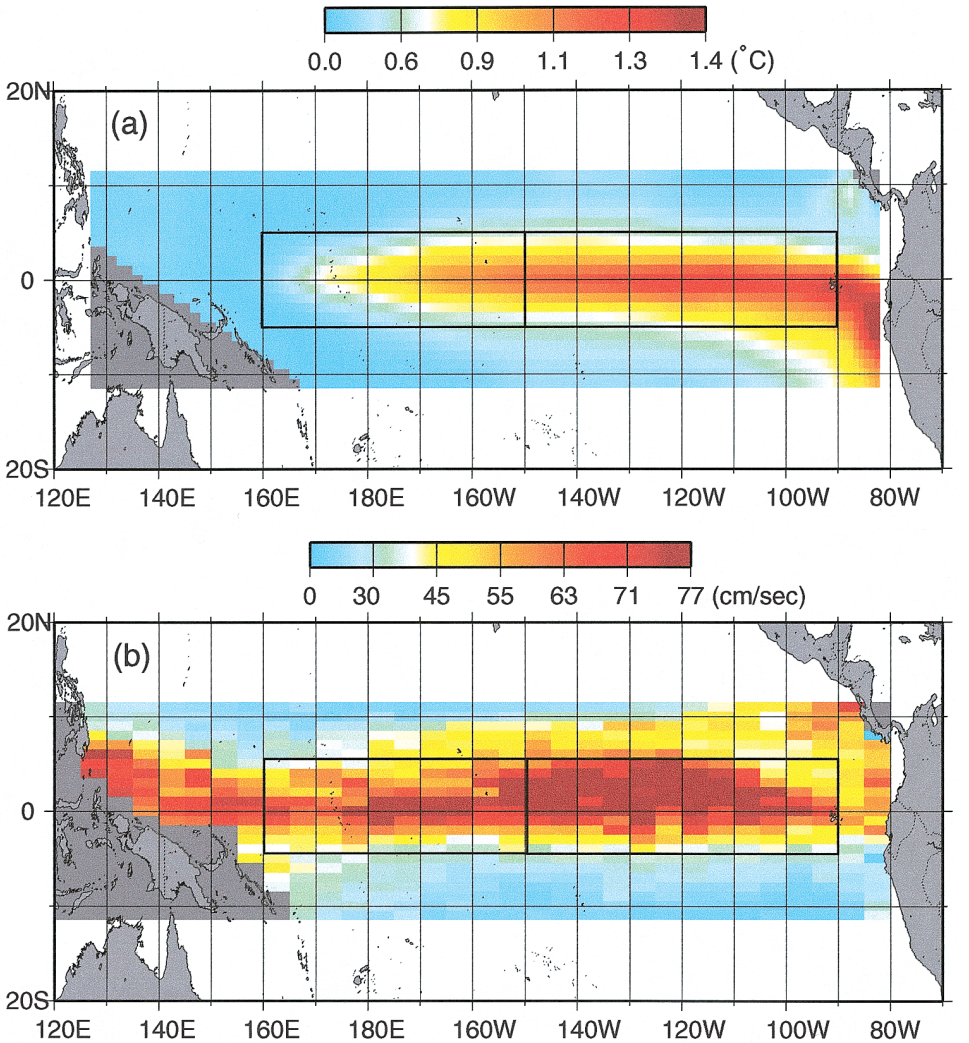

Figure 2. Square root of the variance of 16-month low-passed SST (a) and the variance of the 7-day average velocity (b). Area boundaries of NINO3 (right box) and NINO4 (left box) are solid black lines.

field can effectively be represented by a sum of several principal eigenfunctions of the time average spatial covariance matrix, or EOFs: 4 EOFs can represent the spatial patterns of 80% of the variance shown on Figure 2a (not shown; e.g. Picaut and Busalacchi, 2001).

The rms variance of the 7-day average velocity (Fig. 2b) was largest in the area 2-4N, 150-90W due to Tropical Instability Waves (TIW) that significantly modify the air-sea interaction of the cold tongue (Baturin and Niiler, 1997; Thum *et al.,* 2002). The wind-driven jets are the cause of the secondary velocity rms variance maximum on the

equator at 180-160W (Ralph *et al.,* 1997). For computing the term *C* in Eq. 2, 7-day time series of the velocity were computed at each grid where the SST gradient was computed. The 7-day time series were used because advection is nonlinear and short period variations in two variables when multiplied together can rectify to produce long period variations. To compute these, the 7-day deviations of velocity and temperature gradients were first multiplied together and then low passed to obtain term *C*.

Near-equatorial velocity observations were sparse compared to the SST data, so a velocity interpolation in space and time was done by vector EOFs, computed separately from the SST data. At each location, time mean and monthly mean velocities were computed first. The deviations from these were interpolated to the grid elements using four EOFs of the time average spatial covariance matrix computed from the anomaly velocity observation within 12° of the equator. These four EOF modes account for 31% of the velocity anomaly variance averaged over the entire tropical Pacific basin. Locally, the time variable velocity field in the TIW region was not mapped adequately with the four basin scale EOFs or with the combination of the drifter and current meter data, but 50% of the variance of the wind-driven jets and the countercurrent on the western basin equator were accounted for with four EOFs (not shown).

From previous treatments of observations (Baturin and Niiler, 1997) we can anticipate that the part of the advective convergence, or horizontal mixing, which was related to small spatial and temporal scale processes, were not well represented with our velocity interpolation technique (term *C* of Eq. 2). During the times of strong westerly wind bursts strong eastward flowing jets, with time scales of several days, affect the thermal energy balance within 2°–3° latitude of the equator and 10° of longitude around the dateline (Ralph *et al.,* 1997; Picaut *et al.,* 2001). These equatorially trapped jets move thermal energy from one subregion of NINO4 to another subregion. During the June–November period, the TIWs on weekly time scales produce vigorous horizontal mixing, or advection, of thermal energy across the northern edge of the cold tongue between 150W and 90W (Hansen and Paul, 1984). TIWs move thermal energy from one subregion of NINO3 to another subregion. These 'turbulent' convergences average out spatially over the NINO3,4 regions.

3. The SST balance at NINO3 and NINO4

The 7-day average SST fields and the EOF mapped 7-day average velocity fields were used to compute the local and advective convergence terms on the left-hand side of Eq. 1 during the 1988–2001 time period of contemporaneous velocity and SST observations. The terms *A* and *B* on the right-hand side of Eq. 2 were also computed separately, for which the 16-month band bass data and the time-mean data were used. In NINO4, where the short time-scale velocity field was represented best by the EOF mapping technique, term *C* was an order of magnitude smaller than either of term *A* or *B*. This calculation verified the assertion that wind-driven jets transfer thermal energy from one subregion of NINO4 to another subregion and the net effect averaged out. We were not able to verify in this specific calculation that a more accurate representation of the velocity of term *C* would

contribute to interannual variability to NINO3 region but this was done independently by making an estimate of C from the eddy heat transports presented by Baturin and Niiler (1997; not shown). On the spatial averages of NINO3, which were larger than the scale of the TIWE processes, horizontal thermal energy convergence due to TIWE processes averaged spatially to near zero.

As shown on Figure 3, the largest advective convergence term, in the 1988–2001 period in both NINO3 (96% of the variance of the sum of the terms in Eq. 2) and NINO4 (93% of the variance of the sum of the terms in Eq. 2) was $[\langle V\rangle \cdot \nabla T']$. Thus, using the time-mean velocity defined during 1988–2001, we computed this term for the entire 1981–2001 period when the SST data were available that extended the time series through the 1982–83, 1986–87, 1992–93 and 1997–98 El Ninos. This latter 20-year time series will now be used to test the model of the vertical flux convergence, or the right-hand side of Eq. 1.

The vertical convergence of thermal energy, $[\partial Q/\partial z]'$, is the sum of the turbulent and radiative flux convergences at 15 m depth and is expected to be proportional to the surface values of the same components (as well as the turbulence below the 15 m depth). From the computation of the COADS data, we ascertained that the latent heat flux accounted for most of the variance of the total interannual flux variability (Fig. 5; latent 87.1%, insolation 7.8%, sensible 0.5%, long wave 1.3%). Following Niiler and Krauss (1977), we let $[\partial Q/\partial z]' \cong [Q_0]'/h$, where h is the depth scale of the latent flux convergence, being the well-mixed layer above the tropical thermocline (Moum *et al.,* 1994) and $[Q_0]'$ is the latent surface flux anomaly. We, as others, (e.g. Leeuwenburgh and Stammer, 2001) also found that the SST anomaly is the principal parameter that determined the interannual latent flux anomaly, with the next important parameter being the wind friction velocity, U'_*. The model,

$$[\partial T/\partial t]' + \langle V\rangle \cdot \nabla[T]' = [Q_0]'/c\rho h = -\alpha[T]' - \beta[U_*]', \tag{3}$$

is thus suggested by the above statistical analyses. Thus, in Eq. 3

$$\alpha = (1/c\rho h)(\partial[Q]'/\partial[T]'), \quad \beta = (1/c\rho h)(\partial[Q]'/\partial[U_*]'). \tag{4}$$

We anticipate that such a local balance as suggested by Eq. 3 is not valid in a 2° latitude strip that spans the equator where a model of vertical turbulent flux convergence must also recognize the existence of the time variable turbulence of the undercurrent and $[\partial Q/\partial z]'$, besides being a function of the surface fluxes, must also be a function of the turbulence levels of the undercurrent. However, the area of this strip is small compared to the areas of NINO3,4 and, as is demonstrated below, Eq. 3 captures the large spatial-scale average evolution of both NINO3,4 regions.

A least-square joint regression of the terms on the right-hand side of Eq. 3 was made on the terms on the left-hand side, with 86% of the variance accounted for in NINO3 and 83% in NINO4. The dependence of the latent flux in the combined NINO3,4 areas on $[T]'$ and

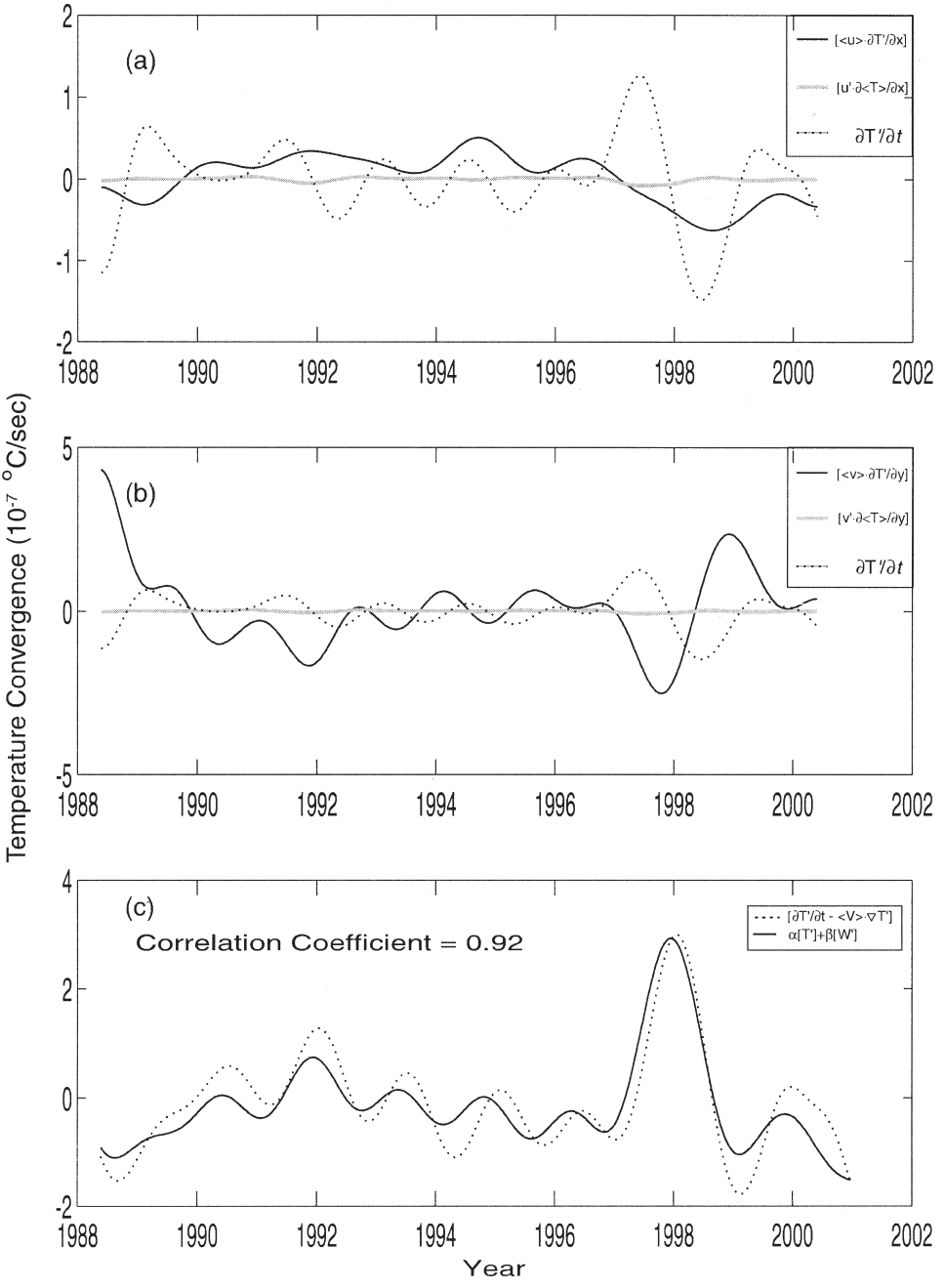

Figure 3. Terms of the thermal energy balance of Eq. 2 in NINO3 region during observation time series of basin scale velocity. Panel (a) depicts the eastward advective component relative to the local convergence component, panel (b) compares the northward advective component and on panel (c) the sum of the local and advective convergences of SST′ is compared to the model of the anomaly of the local turbulent convergence. Please see the text for definitions of the variables.

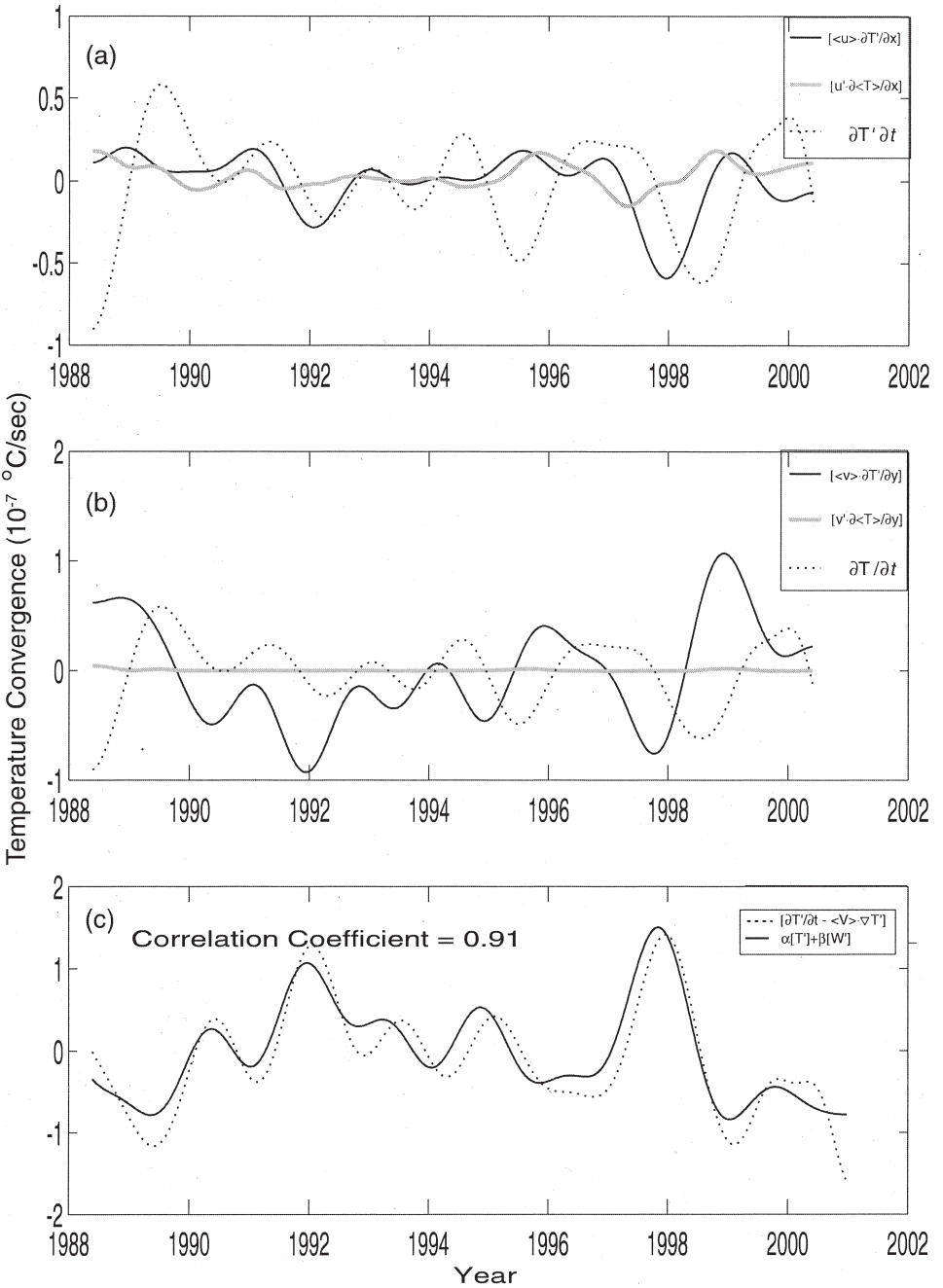

Figure 4. Same as Figure 3, but for NINO4 region.

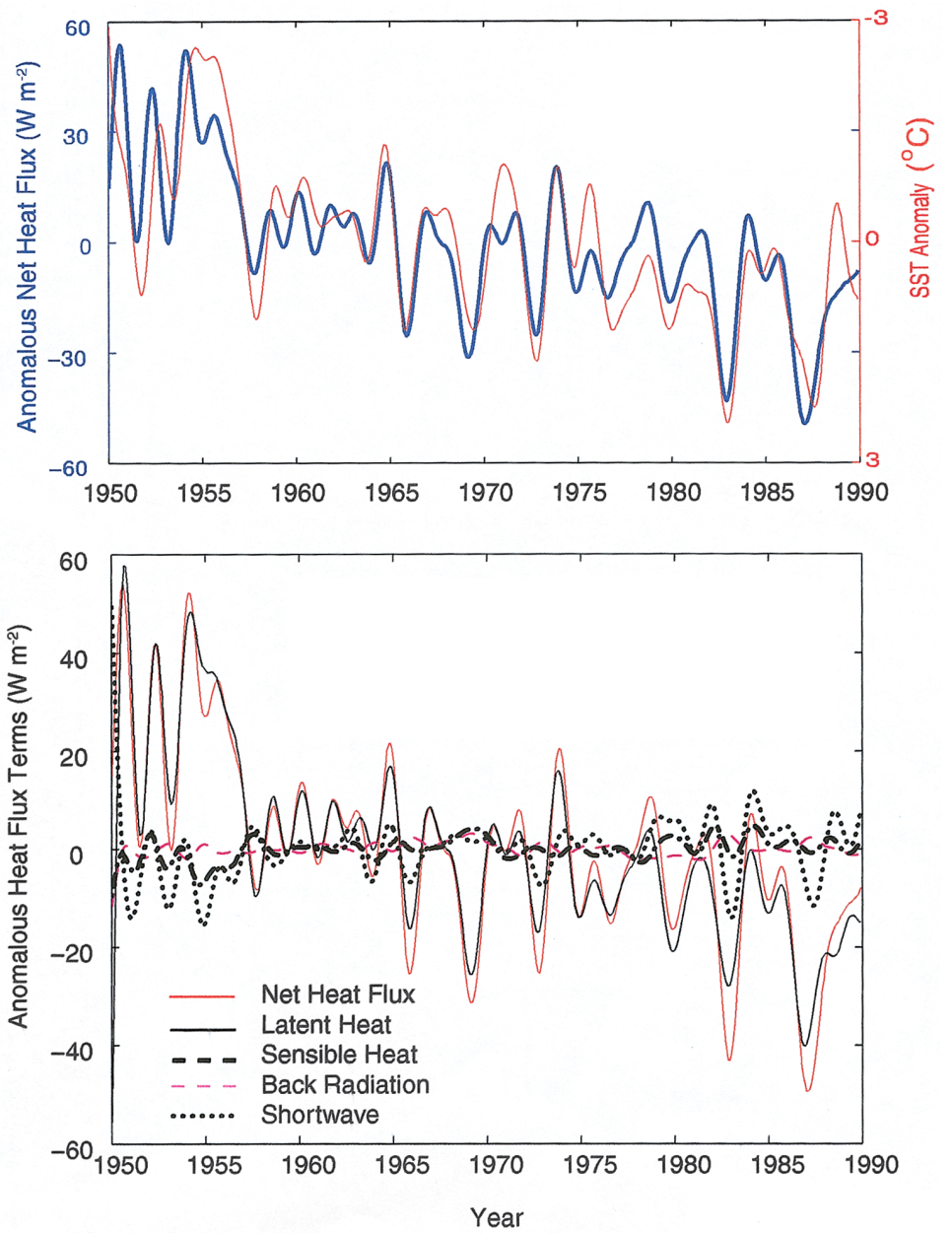

Figure 5. The upper panel displays the NINO3 + NINO4 area average surface heat flux anomaly (right scale) and the SST′ anomaly (left scale). The lower panel displays the individual components of the heat flux anomaly together with the net flux anomaly.

$[U_*]'$ were 20 (w/m^2 C°) (with 78% correlation) and 69 (w/m^2 m sec^{-1}) (with 39% correlation), respectively. The parameters for Eq. 3 were:

NINO3: $\alpha = 0.92\ (\pm.02) \times 10^{-7}$ sec^{-1};

$$\beta = 0.63\ (\pm 0.20) \times 10^{-7}\ \text{sec}^{-1}(\text{C°/m sec});\ h = 61\ (\pm 2)\ \text{m}$$

NINO4: $\alpha = 0.61\ (\pm.02) \times 10^{-7}$ sec^{-1};

$$\beta = 0.75\ (\pm 0.40) \times 10^{-7}\ \text{sec}^{-1}(\text{C°/m sec});\ h = 80\ (\pm 4)\ \text{m}$$

From the time series plots on Figure 6 it is evident that the above analysis captures the large spatial-scale interannual thermal energy balance variability of the equatorial Pacific through the past 20 years. Note that the turbulence convergence depth or the well-mixed layer in the eastern Pacific in this calculation is found to be significantly smaller than in the western Pacific, in concert with observations (e.g. Ralph *et al.,* 1997). Addition of insolation anomaly convergence as a parameter on the right-hand side of Eq. 3 did not improve the amount of variance accounted for on the left-hand side. We found that the principal mechanisms that maintain thermodynamic balance for SST are in decreasing order of their magnitude in variance: (1) advective convergence of thermal energy by the time-mean velocity, (2) vertical mixing of turbulent latent flux component from the atmosphere and (3) local convergence or the local change in temperature. The local convergence, $[\partial T/\partial t]'$, was not shown separately, but its variance was 28% of advection in NINO3 and 36% in NINO4. This balance suggests a rather simple perspective for how El Nino events evolved in the upper ocean in the past 20 years on the large spatial scales: the poleward advection of the anomaly patterns of SST by the time mean surface currents, which are predominantly wind driven, dominated the SST evolution process over most of the tropical Pacific.

To further elucidate the El Nino evolution that is suggested by the analysis that led to Figure 5, consider that Eq. 3 now applies locally everywhere in NINO3, except right on the equator. On the equator the mean flow is very weak (Fig. 1) and this balance is not appropriate. In NINO3 the changes of the surface flux are not related significantly (5%) to the wind speed changes and the advective convergence by the time-mean velocity (term A on the right-hand side of Eq. 2) accounted for 99% of the sum of all other terms.

The simplest, local balance equation in the region 1° latitude poleward from the equator in the eastern tropical Pacific now is:

$$\partial T'/\partial t + \langle v \rangle \partial T'/\partial y = -\alpha T'. \tag{5}$$

The analytic solution to Eq. 5 is:

$$T' = T'_o(t - \zeta;\ x)\ \exp(-\alpha\zeta), \quad \zeta = \int_0^y \{1/\langle v(y;\ x)\rangle\} dy', \tag{6}$$

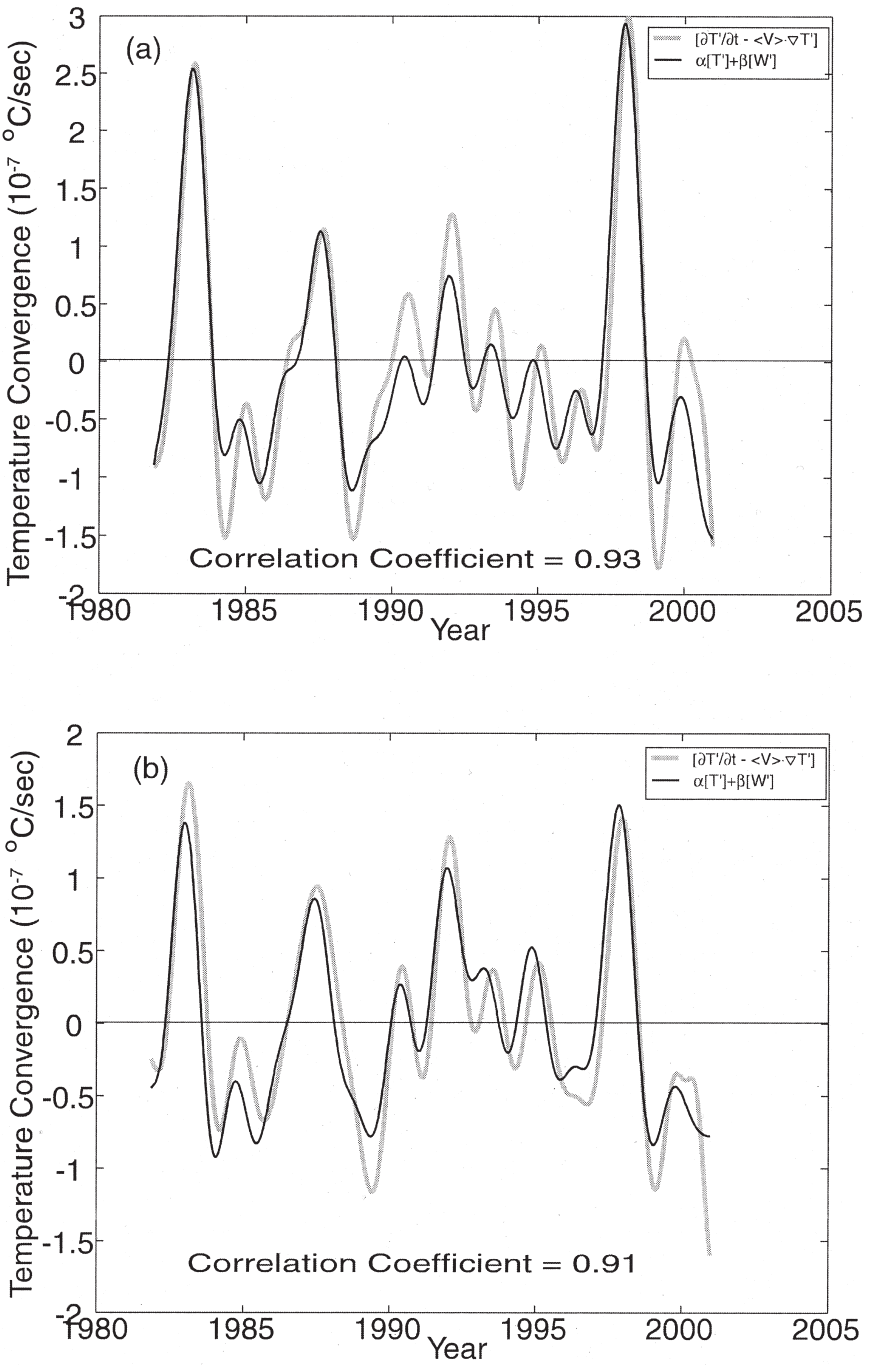

Figure 6. The NINO3 and NINO4 balance of SST′ as expressed in Eq. 3 for the observation time of the SST′ time series.

where $T'_o(t; x)$ is the interannual SST′ specified as a 2° latitude × 5° longitude average centered on the equator and $\langle v(x, y)\rangle$ is the northward component of the time-mean velocity as a function of longitude, x, and latitude, y. Although this balance was suggested from a very large-scale zonal average, we are testing its application to more local spatial scales. While the TIWs have been shown to be important to the local heat balance on annual to semi-annual time scales (Hansen and Paul, 1984) no such demonstration has been made for the interannual time scale evolution in which we are interested here and our data is not appropriate for evaluating the effect of these phenomena.

Eq. 6 is evaluated starting 1° north and south of the equator, where the northward component of velocity is well defined, to 5° and 10° removed from the equator. The solution describes an SST perturbation "wave" that originates on the equator. Off the equator it "decays" by giving to the atmosphere its excessive thermal energy as it is advected poleward by the equatorially divergent mean current. The spatial scale of the perturbed SST′ is established by the ratio of the poleward current to the time scale, $1/\alpha$, at which excess thermal energy is given back to the atmosphere. The time-average poleward velocity component in the eastern tropical Pacific is about 0.05 m/sec and with $\alpha = 0.92 \times 10^{-7}$ sec^{-1}, the exponential decay-scale of the El Nino perturbation is about 550 km. This agrees well with the distribution of the interannual SST rms variance on Figure 2a. A more general solution than Eq. 6 is possible by method of two-dimensional characteristics, with the integral following the pathline of the time mean two-dimensional flow and the northward component replaced by speed (e.g. Hildebrand, 1958), but this solution was not evaluated here.

The observed fields of $T'_o(t; x)$, $\langle v(x, y\rangle$ and $\alpha = 0.92 \times 10^{-7}$ sec^{-1}, as computed from the area average balance in NINO3, was used to evaluate T' time histories at two locations: 117.5W, 5N and 117.5W, 10S (Fig. 7). The SST anomaly on the equator is larger in amplitude and it leads in time the signal at poleward latitudes, as predicted by Eq. 6. It is evident that the physics embodied in the simple balance of Eq. 6 represents well the off-equatorial development of El Nino in the eastern tropical Pacific. We also evaluated Eq. 6 over the entire 12° latitude extent of our study region and carried out and EOF analysis of this synthetic model data. The first three principal EOFs compared very well in both time series amplitude and spatial structures with the modal structures of the original observations (not shown).

4. Discussion

A model equation for the large spatial average thermal energy balance at 15 m depth was proposed that accounted for the predominant variability of the thermodynamic balance of the four El Ninos in the 1981–2001 period. These observations also demonstrate the mechanisms by which the El Nino SST warm (La Nina cool) pattern is restricted to within 10° latitude of the equator. Following the poleward time-mean wind-driven drift of parcels from the equator, the atmosphere has cooled (warmed) anomalous warm (cool) parcels by the time when these parcels reach the 10° latitude distance from the equator.

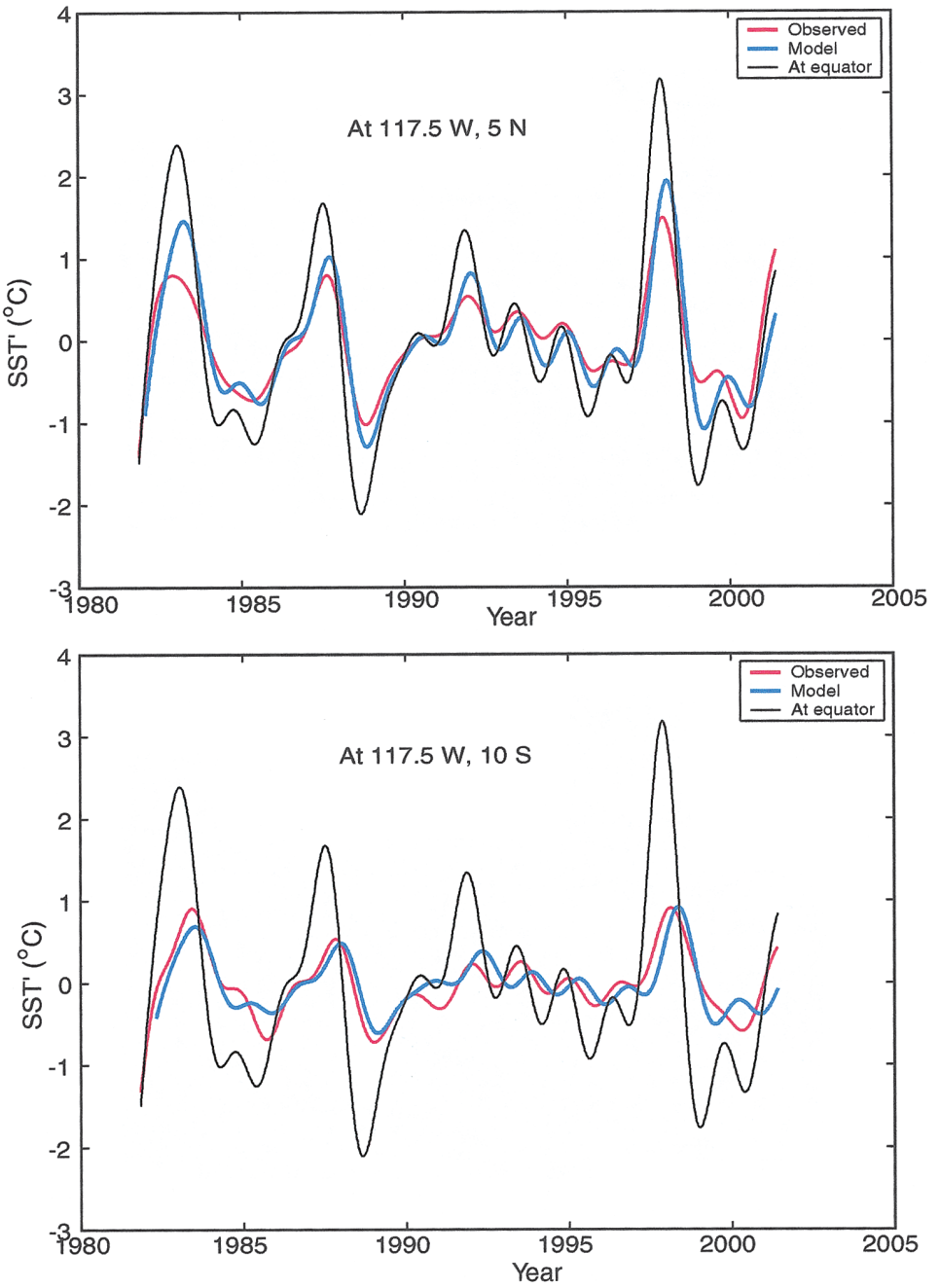

Figure 7. Observed SST′ and SST′ calculated from Eq. 6 along 117.5W.

On the equator the mean velocity was small and term B in Eq. 2 would be larger than term A. The area of the equatorial strip was small compared to the areas of NINO3,4 thus the local imbalance of Eq. 3 caused by our deficiency in modeling the vertical flux convergence to the undercurrent on the equator did not contribute significantly to the area average balances. We note that Suzuki and Takeuchi (2000) analyzed the surface heat balance of an ocean general circulation model of El Nino, in which a realistic component of the wind-driven mean velocity was computed, and came to the same conclusion on the principal terms of the off equatorial local balance as was derived here from observations.

Using moored observations that resolve the vertically integrated heat budget of the upper 50 m of the water column on the equator and the surface heat flux, Wang and McPhaden (2000) showed that a vertical turbulent flux must occur below 50 m that is larger than the surface flux, presumably due to the enhanced vertical turbulence above the core of the equatorial undercurrent. But Wang and McPhaden (2000) did not find a simple parameter with which to express this turbulent flux into the undercurrent.

In an effort to model the turbulent flux into the top of the thermocline, we also included a term on the right-hand side of Eq. 3 that was proportional to the anomalous depth of the 20°C surface. Our hypothesis was that if the thermocline was shallow an increase of vertical mixing of cold water from below would result. We used TAO and drifter velocity and SST data for the period of 1990–2001 at 140W and 110W, together with our SST gradient data to derive the local balances on the left-hand side of Eq. 3. We found no significant improvement over the reduction of its variance that can be obtained by parameterizing the turbulent flux into the top of the undercurrent when it is taken to be inversely proportional to the depth of the main thermocline. Direct observations of circulation with both current meters and with drifters do not support the notion that, following the water motion, interannual SST is getting colder when the interannual depth of the main tropical thermocline on the equator is shallower. Accounting for the El Nino time-scale turbulent flux of heat into the undercurrent will require information on and application of the subsurface velocity and density fields that are beyond the scope of this paper. It is of great importance in the future to understand observationally the processes by which the anomalous SST fields are produced on the equator. The NINO3,4 spatial scale thermal energy balances and the poleward spread and cooling of the anomalous El Nino warm water from the equator were the foci of this paper.

Acknowledgments. The research in this paper was supported at the Scripps Institution of Oceanography by the CORC program of NOAA/OGP under a grant, NA17RJ1231.

REFERENCES

Baturin, N. G. and P. P. Niiler. 1997. Effects of instability waves in the mixed layer of the equatorial Pacific. J. Geophys. Res., *102,* 27,771–27,794.

Bi, K. 1995. Variability of the surface layer circulation in the western equatorial Pacific, Ph.D. Dissertation, University of California at San Diego, CA, 165 pp.

Hansen, D. V. and C. A. Paul. 1984. Genesis and effects of long waves in the equatorial Pacific. J. Geophys. Res., *89,* 10431–10440.

Hildebrand, F. B. 1958. Advanced Calculus for Engineers, Prentice-Hall, Englewood Cliffs, NJ, 245 pp.

Leeuwenburgh, O. and D. Stammer. 2001. The effect of ocean currents on sea surface temperature anomalies. J. Phys. Oceanogr., *31,* 2340–2358.

Moisan, J. R. and P. P. Niiler. 1998. The seasonal heat budget of the North Pacific: Net heat flux and heat storage rates (1950–1990). J. Phys. Oceanogr., *28,* 401–421.

Moum, J. N., D. R. Caldwell and C. A. Paulson. 1994. Mixing in the equatorial surface layer and thermocline. J. Geophys. Res., *94,* 2005–2021.

Niiler, P. 2001. The World Ocean Surface Circulation, *in* Ocean Circulation and Climate: Observing and Modeling the Global Ocean, Chapter 4.1, G. Siedler, J. Church, and J. Gould, eds., Academic Press, London, 715 pp.

Niiler, P. P. and E. B. Kraus. 1977. One-dimensional models of the upper ocean, *in* Modeling and Predication of the Upper Layers of the Ocean, E. B. Kraus, ed., Pergamon Press, NY, 143–172.

Philander, S. G. H. 1990. El Nino, La Nina, and the Southern Oscillation, Academic Press, San Diego, CA, 239 pp.

Picaut, J. and A. J. Busalacchi. 2001. Tropical Ocean Variability, *in* Satellite Altimetry and Earth Sciences, Chapter 4, Academic Press, NY, 217–236.

Picaut, J., M. Ioualalen, T. Delcroix, F. Maisa, R. Murtugudde and J. Vialard. 2001. The oceanic zone of convergence on the eastern edge of the Pacific warm pool: A synthesis of results and implications for El Nino-Southern Oscillation and biogeochemical phenomena. J. Geophys. Res., *106,* 2363–2386.

Ralph, E. A., K. Bi, P. P. Niiler and Y. du Penhoat. 1997. A Lagrangian description of the western equatorial Pacific response to the wind burst of December 1992: Heat advection in the warm pool. J. Climate, *10,* 1706–1721.

Ralph, E. A. and P. P. Niiler. 1999. Wind-driven currents in the tropical Pacific. J. Phys. Oceanogr., *29,* 2121–2129.

Reynolds, A. and T. Smith. 1994. Improved global sea surface temperature analyses using optimum interpolation, J. Climate, *7,* 929–948.

Suzuki, T. and K. Takeuchi. 2000. Response of Equatorial Pacific mean temperature field to intraseasonal wind forcing. J. Oceanogr., *56,* 485–494.

Swenson, M. S. and D. V. Hansen. 1994. Tropical Pacific Ocean mixed layer budget: The Pacific cold tongue. J. Phys. Oceanogr., *29,* 83–91.

Thum, N., S. K. Esbensen, D. B. Chelton and M. J. McPhaden. 2002. Air-sea heat exchange along the northern sea surface temperature front in the eastern tropical Pacific. J. Climate, *15,* 3361–3378.

Wang, W. and M. J. McPhaden. 2000. The surface layer heat balance in the equatorial Pacific ocean, Part II: interannual variations. J. Phys. Oceanogr., *30,* 2989–3008.

Wijffels, S. E., E. Firing and H. Bryden. 1994. Direct observations of the Ekman balance at 10 N in the Pacific. J. Phys. Oceanogr., *24,* 1666–1679.

Received: *26 September, 2003;* revised: *25 August, 2004.*